

## THE *ROSAT*-ESO FLUX-LIMITED X-RAY (REFLEX) GALAXY CLUSTER SURVEY. IV. THE X-RAY LUMINOSITY FUNCTION<sup>1</sup>

H. BÖHRINGER,<sup>2</sup> C. A. COLLINS,<sup>3</sup> L. GUZZO,<sup>4</sup> P. SCHUECKER,<sup>2</sup> W. VOGES,<sup>2</sup> D. M. NEUMANN,<sup>5</sup> S. SCHINDLER,<sup>3</sup>  
G. CHINCARINI,<sup>4</sup> S. DE GRANDI,<sup>4</sup> R. G. CRUDDACE,<sup>6</sup> A. C. EDGE,<sup>7</sup> T. H. REIPRICH,<sup>2</sup> AND P. SHAVER<sup>8</sup>

Received 2001 May 31; accepted 2001 October 15

### ABSTRACT

The X-ray galaxy cluster sample from the REFLEX Cluster Survey, which covers the X-ray brightest galaxy clusters detected in the *ROSAT* All-Sky Survey in the southern sky, is used to construct the X-ray luminosity function of clusters in the local universe. With 452 clusters detected above an X-ray flux limit of  $3 \times 10^{-12}$  ergs s<sup>-1</sup> cm<sup>-2</sup> in 4.24 sr of the sky, this sample is the most comprehensive X-ray cluster sample with a well-documented selection function, providing the best current census of the local X-ray galaxy cluster population. In this paper we discuss the construction of the luminosity function and the effects of flux measurement errors and of variations with sample region, and we compare the results with those from previous surveys.

*Subject headings:* cosmology: observations — galaxies: clusters: general — large-scale structure of universe — X-rays: galaxies

### 1. INTRODUCTION

Because the X-ray luminosity of galaxy clusters is closely related to the cluster mass (Reiprich & Böhringer 1999, 2001) and can be measured for a large sample of galaxy clusters, the X-ray luminosity function provides a good estimate of the mass function of galaxy clusters. Therefore the X-ray luminosity function has been widely used as a census of the galaxy cluster population in the universe (see, e.g., Piccinotti et al. 1982; Kowalski et al. 1984; Gioia et al. 1984; Edge et al. 1990; Henry et al. 1992; Burns et al. 1996; Ebeling et al. 1997; Collins et al. 1997; Burke et al. 1997; Rosati et al. 1998; Vikhlinin et al. 1998; De Grandi et al. 1999; Ledlow et al. 1999; Nichol et al. 1999; Gioia et al. 2001). The close connection of cluster formation with the evolution of the large-scale structure of the universe makes the cluster mass function—and its observational substitutes, the X-ray luminosity function or X-ray temperature function—very important for the statistics of large-scale structure and for tests of cosmological models. The cluster luminosity function constrains in particular the normalization of the amplitude of the primordial density fluctuation power spectrum on scales of about 5 to 10  $h_{100}^{-1}$  Mpc (see, e.g., Henry & Arnaud 1991; Bahcall & Cen 1993; White, Efstathiou, & Frenk 1993), and the evolution of the X-ray luminosity function provides a sensitive test of the mean density of the universe (see, e.g., Perrenod 1980; Oukbir & Blanchard 1992; Eke, Cole, & Frenk 1996; Viana & Liddle 1996; Borgani et al. 1999; Reichart et al. 1999).

A precise measurement of this function had to await the availability of cluster samples large enough to reduce the statistical scatter and effects of cosmic variance and homogeneous enough to minimize uncertainties and corrections of selection effects. The *ROSAT* All-Sky Survey (RASS;

Trümper 1992, 1993), its improved processing (Voges et al. 1999), and a comprehensive optical follow-up observing program provided the basis for the necessary improvements. In this paper we use the *ROSAT*-ESO Flux-Limited X-ray (REFLEX) cluster survey (Böhringer et al. 1998, 2001 [latter is hereafter Paper I]; Guzzo et al. 1999; Collins et al. 2000, hereafter Paper II; Schuecker et al. 2001, hereafter Paper III), comprising 452 southern clusters in total, 449 with measured redshifts, above a nominal X-ray flux limit of  $3 \times 10^{-12}$  ergs s<sup>-1</sup> cm<sup>-2</sup> in the *ROSAT* band (0.1–2.4 keV), to construct the X-ray luminosity function of galaxy clusters in the local universe. Compared with previous cluster samples based on the RASS and used for the construction of the X-ray luminosity function, the present sample is more than a factor of 2 larger and features a well-understood selection function. It provides a good measure of the local luminosity function for studies of cluster evolution by comparison with distant X-ray cluster samples (see, e.g., Gioia et al. 2001).

This paper is organized as follows. Section 2 gives a short description of the REFLEX cluster sample. The flux and luminosity determination is summarized in § 3. In § 4, the X-ray luminosity function is derived, and comparison with previous results is made in § 5. In § 6, we discuss the dependence of the results on the cosmological model adopted for the analysis. Section 7 provides a summary. For the calculation of luminosities and volume we use the cosmological parameters  $H_0 = 50$  km s<sup>-1</sup> Mpc<sup>-1</sup>,  $\Omega_0 = \Omega_m = 1$ , and  $\Lambda = 0$ , or alternatively,  $\Omega_m = 0.3$  and  $\Omega_\Lambda = \Lambda/3H_0^2 = 0.7$ .

### 2. THE REFLEX CLUSTER SAMPLE

The construction of the REFLEX cluster sample is described in detail by Paper I. The survey area covers the southern sky up to the declination  $\delta = +2^\circ.5$ , avoiding the band of the Milky Way ( $|b_{\text{II}}| \leq 20^\circ$ ) and the regions of the Magellanic clouds. The total survey area is 13,924 deg<sup>2</sup> or 4.24 sr.

The X-ray detection of the clusters is based on the second processing of the RASS (Voges et al. 1999), providing 54,076 sources in the REFLEX area. All sources were reanalyzed by means of the growth curve analysis (GCA) method (Böhringer et al. 2000), and the results are used to produce a

<sup>1</sup> Based on observations at the European Southern Observatory, La Silla, Chile.

<sup>2</sup> Max-Planck-Institut für extraterrestrische Physik, D-85740 Garching, Germany.

<sup>3</sup> Liverpool John Moores University, Liverpool, UK.

<sup>4</sup> Osservatorio Astronomico di Brera, Merate, Italy.

<sup>5</sup> CEA Saclay, Service d'Astrophysique, Gif-sur-Yvette, France.

<sup>6</sup> US Naval Research Laboratory, Washington, DC 20375.

<sup>7</sup> Physics Department, University of Durham, Durham, UK.

<sup>8</sup> European Southern Observatory, Garching, Germany.

flux-limited sample of RASS sources with a nominal flux of  $F_n \geq 3 \times 10^{-12}$  ergs s<sup>-1</sup> cm<sup>-2</sup> (with  $F_n$  as defined below). Cluster candidates were found using a machine-based correlation of these X-ray sources with galaxy density enhancements in the COSMOS optical database (derived from digital scans of the UK Schmidt survey plates by COSMOS at the Royal Observatory Edinburgh; MacGillivray & Stobie 1984). The resulting candidate list was carefully screened, based on X-ray and optical information, literature data, and results from the optical follow-up observation program. The selection process was designed to provide a completeness in the final cluster catalog in excess of 90% with respect to the flux-limited sample of GCA-selected RASS sources. This high completeness of the cluster identification of the RASS sources ensures that the selection effects introduced by the optical identification process are minimized and negligible for our purpose (see also statistics given in Paper I). Further tests provide support that this value of >90% also describes the general completeness of the flux-limited cluster sample in the survey area. For example, an independent search for X-ray emission for the clusters cataloged by Abell, Corwin, & Olowin (1989) returns only one supplementary cluster with a flux above the flux limit that has not been included in the REFLEX sample. In addition, tests based on the Galactic latitude, redshift, and photon count distribution, as well as on an independent screening of all significantly extended RASS X-ray sources in the survey region, are well consistent with this claim (Paper I; Paper III). Based on the X-ray spectral properties of the REFLEX cluster sources, we can also estimate that fewer than 9% of the X-ray cluster sources have a strong X-ray flux contributions from active galactic nuclei (AGNs; Paper I).

The final cluster sample comprises 452 objects, including three uncertain candidates without redshifts. (Further optical work has so far not provided further evidence that these sources are clusters: one object is tentatively identified as BL Lac object, one is probably a collection of three or four point sources, and the third source is pointlike, with no cluster seen on deeper CCD images. Details on the identifications will be given in the forthcoming catalog paper). These three objects are excluded from further analysis. The sample has already been used to analyze the statistics of the spatial cluster distribution with the two-point correlation function (Paper II) and with the density fluctuation power spectrum (Paper III).

### 3. LUMINOSITY AND SURVEY VOLUME DETERMINATION

The X-ray luminosities of the REFLEX clusters are determined from the count rate measurements provided by the GCA (Böhringer et al. 2000). For the first analysis, these count rates are not corrected by means of a model estimate of the total flux. Such modifications are discussed in a second step. To determine the cluster X-ray luminosity, we convert the measured count rate into a “nominal” X-ray flux for the ROSAT band (0.1–2.4 keV),  $F_n$ , by assuming a Raymond-Smith-type spectrum (Raymond & Smith 1977) for a temperature of 5 keV, a metallicity of 0.3 of the solar value (Anders & Grevesse 1989), a redshift of zero, and an interstellar hydrogen column density as found for the line of sight in the compilation by Dickey & Lockman (1990), as given within EXSAS (Zimmermann et al. 1994). The value of  $F_n$  is used to make the flux cut independent of any redshift information (because the redshift is not available for all

objects at the start of the survey). With the redshift value at hand, the X-ray flux is redetermined ( $F_X$ ) with an improved spectral model, where the temperature is now estimated (iteratively) from the preliminarily derived X-ray luminosity and the luminosity-temperature relation (uncorrected for cooling flow effects) derived by Markevitch (1998). The redshift of the spectrum is now taken into account by folding a redshifted spectrum with the instrument response, which is similar to a  $k$ -correction, with  $k(T, z, N_H)$ , and provides luminosities for the cluster rest-frame energy band 0.1–2.4 keV.

For the construction of the luminosity function of a flux-limited sample, the survey volume,  $V_{\max}$ , as a function of X-ray luminosity has to be known. The survey volume is given by the volume of the cone defined by the survey area and the luminosity distance at which a cluster with a given luminosity could just be observed at the flux limit. Because we have used the flux parameter  $F_n$  for the flux cut  $F_{n \text{ lim}}$ , we have to determine the maximum luminosity distance,  $D_{L \text{ lim}}$ , for the parameter  $L_X$  under the assumption that the flux is determined for a 5 keV spectrum at  $z = 0$ . Because we have calculated the luminosity,  $L_X$ , iteratively from  $F_n$ , we have to reverse these steps to determine the limiting luminosity distance,  $D_{L \text{ lim}}$ , from  $L_X$ , given  $F_{n \text{ lim}}$ . This is iteratively calculated from  $F_{n \text{ lim}}$  and  $L_X$  involving the two steps:

$$\text{corr} = F_{X \text{ lim}}/F_{n \text{ lim}} = f(L_X, D_{L \text{ lim}}), \quad (1)$$

$$D_{L \text{ lim}}^2 = \frac{L_X}{4\pi F_{n \text{ lim}} \text{corr}(L_X, D_{L \text{ lim}})k(T, z, N_H)}. \quad (2)$$

These equations establish a unique relation between  $L_X$  and  $V_{\max}$  for a given  $F_{n \text{ lim}}$ . The two correction factors are small, with typical values quoted by Böhringer et al. (2000); that is, the difference between  $F_n$  and  $F_X$  is only a few percent, except for the low-luminosity systems, where it is larger. (Note that no new flux cut has been introduced after the correction of the flux values. Therefore the sample does not change, and the selection volume depends on  $F_{n \text{ lim}}$ ).

The second correction applied in the  $V_{\max}$  calculation concerns the sensitivity function derived in Paper I, providing the sky coverage as a function of flux (Paper I, Figs. 22 and 23). The sensitivity function is defined by two limiting parameters: the flux limit,  $F_{n \text{ lim}}$ , and the minimum number of photons required for a safe detection and flux measurement. We use a soft coding of the photon number cut, such that the effect of using different cut values can easily be explored. For a minimum value of 10 photons, for example, the nominal flux limit is reached in 97% of the REFLEX area, while for a value of 30 photons this fraction is 78%. For the remaining part of the sky with higher flux limit, the corresponding survey volume has to be reduced accordingly. The large sample size of REFLEX allows us to be selective and to use the very safe, higher cut of 30 photons for the standard derivation of the luminosity function.

As shown in Paper I, a complete removal of the photon number cut leads to an estimated deficit of only about  $14 \pm 7$  clusters (3.8%). Thus, the assumption of a homogeneous selection function without source count limit and inclusion of all clusters lead to results insignificantly different from the results obtained with the conservative approach below. For a minimal photon number of 30, the sample contains 423 clusters with redshifts. For luminosities lower than  $L_X = 10^{42}$  ergs s<sup>-1</sup>, the counterparts to the extended X-ray sources very often appear as single elliptical

galaxies with no optically bright companions, and therefore these objects may be incompletely represented in our sample. We therefore exclude three objects with lower luminosity from the parametric fit to the luminosity function described below.

#### 4. RESULTS

The binned luminosity function calculated for this sample is shown in Figure 1 (with 20 clusters per bin). The three objects with the lowest luminosity are grouped here into the first bin. The calculation for each bin uses the formula

$$n(L) = \frac{1}{\Delta L} \sum_{i=1}^N \frac{1}{V_{\max}(L_i)}, \quad (3)$$

where the sum is over all  $N$  clusters falling into the luminosity interval of the bin. Note that with this approach we determine the mean luminosity function in the survey volume, averaging over large-scale structure density fluctuations. Also, no major redshift dependence of the cluster density has been detected. An alternative determination of a density-independent luminosity function and the redshift dependence of the cluster density is planned for a future paper. The error bars shown are Poissonian errors based on the number of clusters per bins. The function shown by circles concerns the observed fluxes only. To explore the effect of the flux missed by the GCA algorithm in the outskirts of the clusters, we correct the fluxes and luminosities on the basis of a self-similar cluster model, as described in Böhringer et al. (2000): a  $\beta$  model (Cavaliere & Fusco-Femiano 1976) with a  $\beta$ -value of  $\frac{2}{3}$ , a core radius that scales with mass, and an assumed extent of the X-ray halo out to 12 times the core radius. The correction procedure has been successfully tested by simulations based on the same cluster model. The resulting corrected luminosity function is also shown in Figure 1. As expected from the typical mean correction factor of about 8% (Böhringer et al. 2000), the main effect is a shift of the curve to higher luminosity of this order. A larger shift is only observed for the lowest-redshift bins (for the groups with extended, low surface brightness

emission). The numerical values for the data points shown in this and some of the following plots are given in Tables 2–7 in the Appendix. There we also provide the data for the REFLEX luminosity function for the 0.5–2.0 keV energy band.

As a first consistency check, we compared luminosity functions derived for flux limits of  $3 \times 10^{-12}$  and  $5 \times 10^{-12}$  ergs  $s^{-1} \text{ cm}^{-2}$ , finding excellent agreement. This indicates that there is no significant incompleteness effect at low fluxes. We also derived an unbinned, parametric representation of the luminosity function in the form of a Schechter function

$$n(L)dL = n_0 \exp\left(-\frac{L}{L_*}\right) \left(\frac{L}{L_*}\right)^{-\alpha} \frac{dL}{L_*} \quad (4)$$

(Schechter 1976), by means of a maximum likelihood (ML) approach, following Murdoch, Crawford, & Jauncey (1973),

$$\mathcal{L} = -N \ln K + \sum_i \ln [V_{\max}(L_i)n(L_i)], \quad (5)$$

with

$$K = \int_{L_{\min}}^{\infty} dL V_{\max}(L)n(L), \quad (6)$$

where  $\mathcal{L}$  is the log-likelihood value, and by a Poisson formulation of the ML method

$$\mathcal{L} = -K + \sum_i \ln [V_{\max}(L_i)n(L_i)], \quad (7)$$

where  $N$  is the total number of clusters in the sample (see, e.g., Daley & Vere-Jones 1988). Both methods can be considered a compatibility test of the observed luminosity distribution function,  $V_{\max}(L)n(L)$ , with the model expectation. We obtained identical results with both approaches. The integral and the summation in the above equations are taken over the luminosity range  $10^{42}$  ergs  $s^{-1}$  to infinity. The resulting best-fit parameters are given in Table 1. The normalization parameter,  $n_0$ , is derived from the requirement that the total number obtained by integration of  $n(L)$  equals the observed number of clusters. The constraints obtained from the maximum likelihood analysis for the shape parameters are shown in Figure 2. We have also

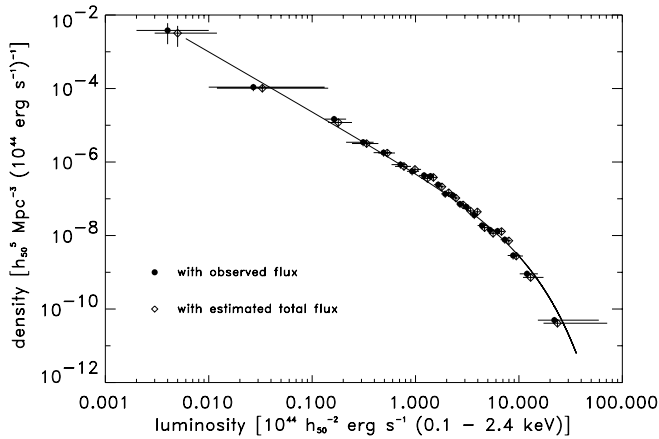


FIG. 1.—X-ray luminosity function for the REFLEX sample. *Circles*: Results for the detected luminosities; *diamonds*: results including a model-dependent correction for the missing flux. Data points are plotted at the density-weighted mean luminosity per bin. The line gives the maximum likelihood fit, including the correction for missing flux and the individual uncertainties in the flux measurement. The horizontal bars indicate the bin width and the vertical error bars, which hardly exceed the size of the symbols, give the Poissonian uncertainties of the cluster counts in each bin. Numerical values of the data points are listed in Tables 2 and 3.

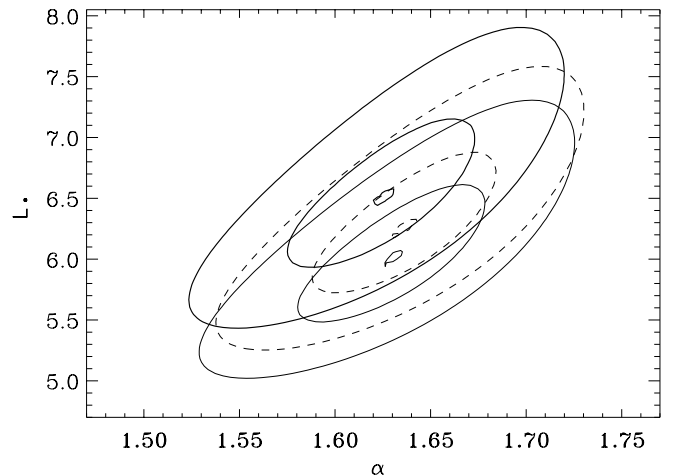


FIG. 2.—Constraints on the parameters of the shape of the Schechter function derived from maximum likelihood fits to the total sample. *Thick solid lines*: Fits including corrections for missing flux and flux errors; *thin solid lines*: fits uncorrected for missing flux; *dashed lines*: fits with no correction for missing flux or flux error. Contour lines encircle the best-fitting values and indicate the  $1 \sigma$  and  $2 \sigma$  limits, respectively.

TABLE 1  
RESULTS OF THE FITTING OF A SCHECHTER FUNCTION TO REFLEX X-RAY LUMINOSITY FUNCTION AND  
RESULTS FROM PREVIOUS WORK

Sample	$L_*$ <sup>a</sup> ( $10^{44} h_{50}^{-2} \text{ ergs s}^{-1} \text{ cm}^{-2}$ )	$\alpha$	$n_0$ ( $h_{50}^3 \text{ Mpc}^{-3}$ )
REFLEX uncorrected .....	$6.26^{+0.6}_{-0.53}$ <sup>b</sup>	$1.63 \pm 0.06$	$(1.75^{+0.5}_{-0.4}) \times 10^{-7c}$
REFLEX uncorrected <sup>d</sup> .....	$8.0^{+0.8}_{-0.7}$ <sup>b</sup>	$1.70 \pm 0.045$	$1.31 \times 10^{-7}$
Corrected for missing flux .....	$6.79^{+0.6}_{-0.55}$	$1.63 \pm 0.06$	$(1.80^{+0.5}_{-0.4}) \times 10^{-7}$
Corrected for flux error .....	$6.00^{+0.6}_{-0.5}$	$1.63 \pm 0.06$	$(1.58^{+0.5}_{-0.4}) \times 10^{-7}$
Corrected for flux error <sup>d</sup> .....	$7.61 \pm 0.8$	$1.69 \pm 0.045$	$1.20 \times 10^{-7}$
Corrected for both effects .....	$6.47^{+0.6}_{-0.53}$	$1.63 \pm 0.06$	$(1.68^{+0.5}_{-0.4}) \times 10^{-7}$
Corrected for both effects <sup>d</sup> .....	$8.36^{+0.9}_{-0.8}$	$1.69 \pm 0.045$	$1.07 \times 10^{-7}$
High-flux sample uncorrected <sup>e</sup> .....	$6.85 \pm 0.7$	$1.68 \pm 0.07$	$(1.5^{+0.6}_{-0.5}) \times 10^{-7}$
REFLEX south <sup>f</sup> .....	$5.04^{+0.7}_{-0.5}$	$1.55 \pm 0.07$	$2.6 \times 10^{-7}$
REFLEX north <sup>f</sup> .....	$9.4^{+1.9}_{-1.6}$	$1.79 \pm 0.07$	$0.9 \times 10^{-7}$
BCS .....	$9.1^{+2.0}_{-1.5}$	$1.85 \pm 0.09$	$(7.74^{+0.76}_{-0.70}) \times 10^{-8}$
RASS1 BS .....	$6.08^{+1.1}_{-0.9}$	$1.52 \pm 0.11$	$(2.53 \pm 0.23) \times 10^{-7}$
Ledlow et al. 1999 .....	$8.78 \pm 0.62$	$1.77 \pm 0.01$	$(7.9 \pm 0.38) \times 10^{-8}$

<sup>a</sup>  $L_*$  is measured in the 0.1–2.4 keV band.

<sup>b</sup> Errors are quoted for 68% limits.

<sup>c</sup> The errors quoted for the normalization for the REFLEX samples were evaluated by a  $\chi^2$  method with two free parameters ( $L_*$ ,  $\alpha$ ), which differs from the approach for the other samples. For one free parameter the error reduces to  $\pm 0.1$  to  $\pm 0.2$  and to  $\pm 0.08$  for fixed ( $L_*$ ,  $\alpha$ ) and Poissonian errors.

<sup>d</sup> For noncritical density cosmology with  $\Omega_m = 0.3$  and  $\Omega_\Lambda = 0.7$ .

<sup>e</sup> Sample with a flux limit of  $5 \times 10^{-12} \text{ ergs s}^{-1} \text{ cm}^{-2}$ .

<sup>f</sup> Uncorrected for flux error and missing flux.

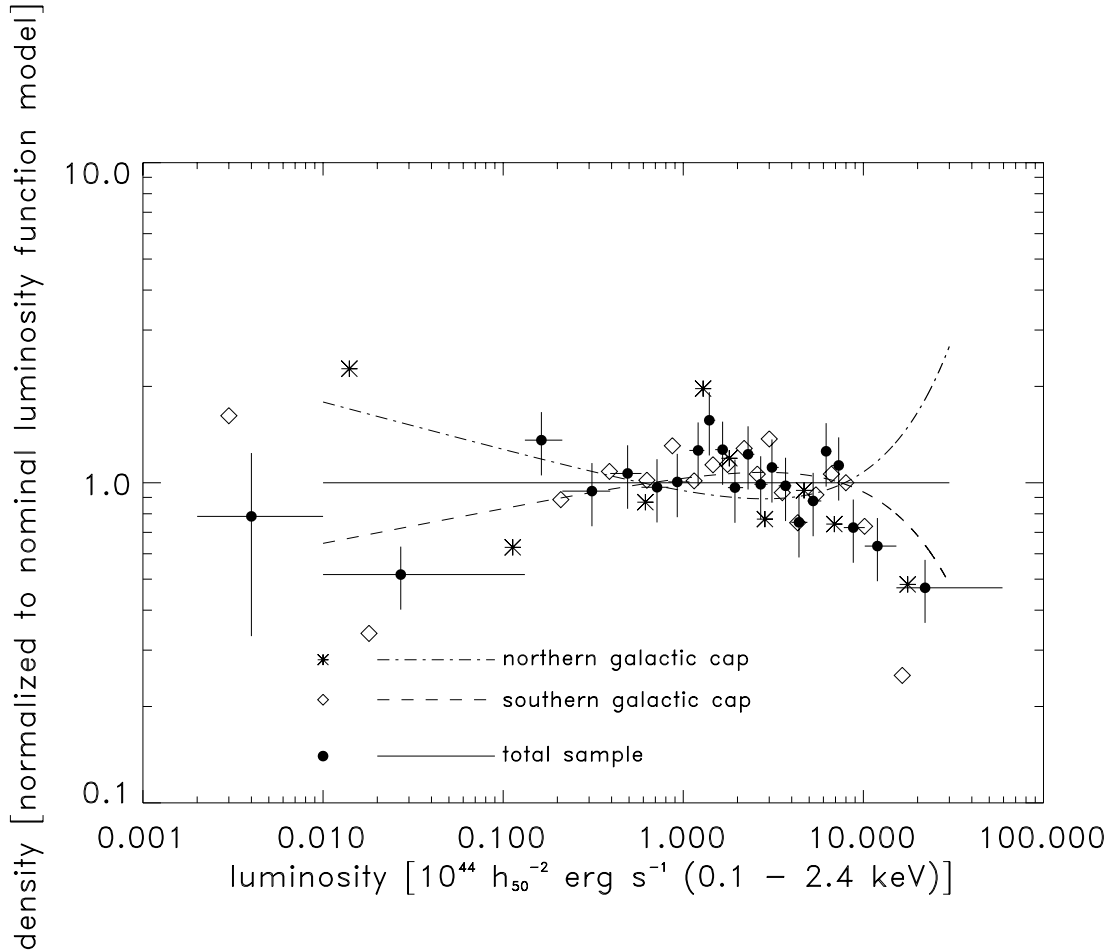


FIG. 3.—Comparison of the X-ray luminosity function derived for the subsamples in the southern and northern Galactic caps with the results for the total REFLEX sample. All results are normalized by the luminosity function for the total sample (solid line;  $L_* = 6.26$ ,  $\alpha = 1.63$ ,  $n_0 = 1.75 \times 10^{-7}$ ). All functions are given in the observed, uncorrected form. Numerical values for the data points shown in this plot are given in Tables 4 and 5.

performed a  $\chi^2$  fit to the binned data to test for the quality of the fit and obtained  $\chi^2$ -values of 18 (for 19 dof, 22 bins), 39 (for 40 dof, 43 bins), and 64 (for 68 dof, 71 bins). Thus, the Schechter function provides a good representation of the data within the current uncertainty limits. The  $\chi^2$  method is also used for the error estimation for  $n_0$ .

In the next step of the analysis we consider the effect of the uncertainties in the flux measurement on the results. The uncertainty in the flux measurement has two effects: the luminosity of a cluster can be overestimated (underestimated), and at the same time the maximum detection volume is pushed to larger (smaller) size for a given luminosity. The survey volume effect is equivalent to the Eddington bias (Eddington 1940). Therefore, the expectation function for the luminosity distribution in the likelihood approach,  $V_{\max}(L)n(L)$ , has to be folded with the error probability function. To account for this effect, we extend the maximum likelihood approach of Murdoch et al. (1973) to include the effect of errors on the expected luminosity distribution, as well as on the uncertainty of the survey volume. The log-likelihood,  $\mathcal{L}$ , is then given by

$$\mathcal{L} = \sum_i \left[ -\ln K(\sigma_i) + \ln \int_{L_{\min}}^{\infty} V_{\max}(L)n(L)G(L_i, L, \sigma_i)dL \right], \quad (8)$$

with

$$K(\sigma_i) = \int_{L_{\min}}^{\infty} dL \int_{L_{\min}}^{\infty} dL' V_{\max}(L)n(L)G(L, L', \sigma_i), \quad (9)$$

where  $G(L, L', \sigma_i)$  is a normalized Gaussian distribution containing the photon noise error of the flux measurement,  $\sigma_i$ , for each cluster and the sum is over all clusters in the sample. A similar modification can be introduced into the approach defined by equations (5) and (6), yielding again the same results as the formalism of equations (8) and (9). While the previous correction for missing flux leads essentially to an increase in  $L_*$  of about 8%, the inclusion of the flux errors results in a decrease of about 4%. Both effects are relatively small, yielding overlapping parameter constraints (Fig. 2).

As another test of the stability of the results, we compare in Figure 3 and Table 1 the results obtained for the luminosity function when the REFLEX sample is split into the parts above and below the Galactic disk. Because the differences in the compared luminosity functions are difficult to notice in the usual display of the luminosity function, where the amplitude dimension extends over several orders of magnitude (as seen in Fig. 1), we have chosen a different representation here. In Figure 3, we divide all functions to be compared by the Schechter function that provided the best fit to the complete REFLEX sample. In this way we

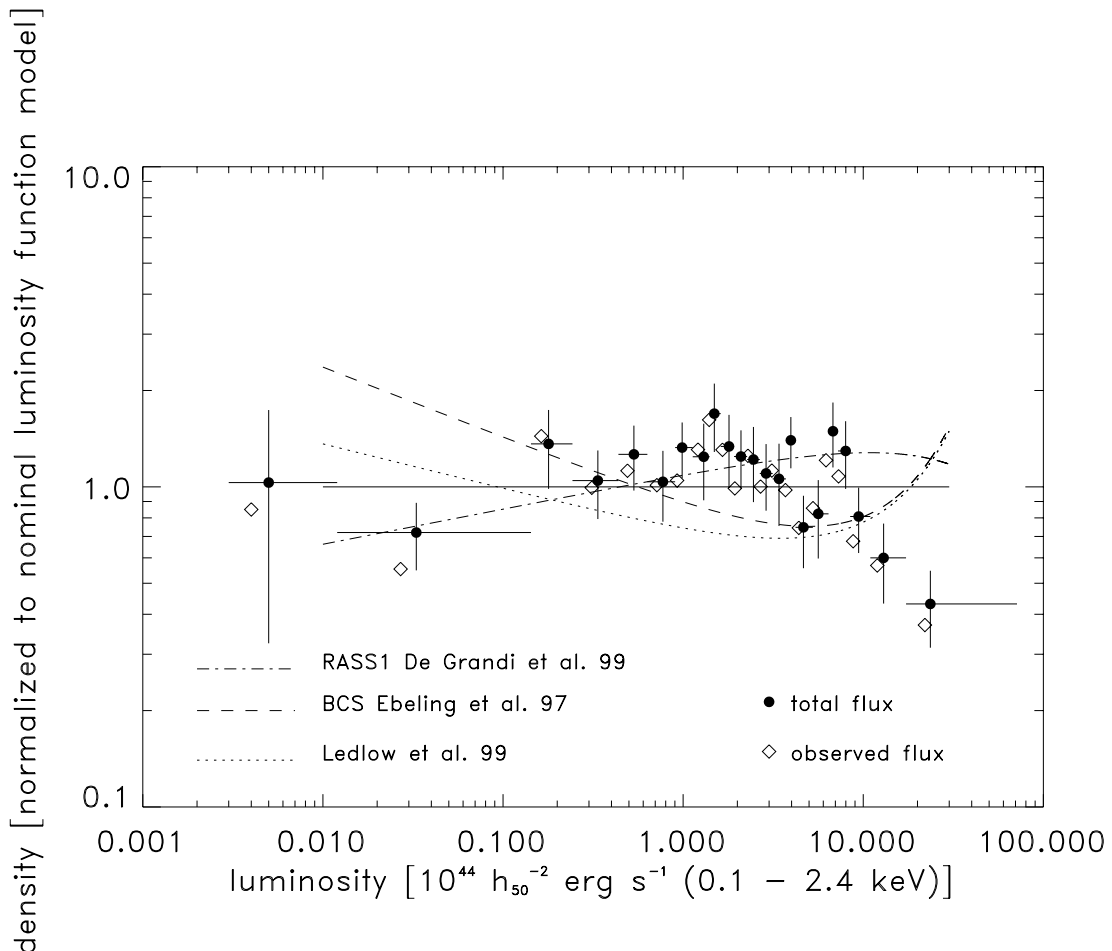


FIG. 4.—Comparison of the REFLEX X-ray luminosity function with those of the BCS (Ebeling et al. 1997), the RASS1 Bright Sample (De Grandi et al. 1999), and X-ray-detected Abell clusters (Ledlow et al. 1999). All results are normalized by the luminosity function for the REFLEX sample (solid line;  $L_* = 6.79$ ,  $\alpha = 1.63$ ,  $n_0 = 1.8 \times 10^{-7}$ ). The REFLEX function is used in the form corrected for missing flux but uncorrected for the flux errors, to conform with the treatment of the other surveys. The REFLEX data points without missing flux correction are also shown.

display only the differences, and the best-fitting model function is represented by a horizontal line in this plot.

There is good agreement within the error bars at intermediate luminosities, where most of the clusters were found. The deviations at low luminosities are consistent with the cosmic variance estimated for the respective survey volume (approximated to be spherical) and the power spectrum determined for the REFLEX cluster distribution (Paper III). Details of the estimate of the cosmic variance will be given in a further publication in this series. The differences at the highest luminosity are due to small number statistics.

## 5. COMPARISON WITH PREVIOUS RESULTS

In Figure 4 we compare the results for REFLEX with the largest previous samples from the first processing of the RASS, our RASS1 Bright Sample (BS) in the south (De Grandi et al. 1999), Brightest Cluster Sample (BCS) in the north (Ebeling et al. 1997), and the work by Ledlow et al. (1999) based on X-ray detections of Abell clusters (all richness classes). We note that, even though the results agree within the combined individual errors in this binned representation, there are global differences. At low luminosities the differences are approximately within the expected cosmic variance (e.g., Fig. 3). The low density at low luminosities in the Ledlow et al. sample is due to the fact that the Abell catalog does not sample well the X-ray-emitting galaxy groups. At medium luminosity, around  $L_x = (4-10) \times 10^{44}$  ergs  $s^{-1}$ , where the data sets are most accurate, the results for the RASS BS are systematically higher, and the BCS and Ledlow et al. sample are lower by about 20%–30%. The De Grandi et al. results predict a cluster density for the most interesting part of the luminosity function about 50% higher than that of the BCS (noted also by Gioia et al. 2001 in their comparison of the BCS, RASS BS, and REFLEX surveys to the distant north ecliptic pole [NEP] sample). This comparison shows in which respect an improvement in the precision of the luminosity function constitutes important progress: it provides a better reference for the local universe in the study of cluster evolution.

## 6. RESULTS FOR $\Lambda$ COSMOLOGIES

Because there is increasing evidence that the geometry of the universe is described by a nonzero cosmological parameter, with one of the most likely models being characterized by a density parameter,  $\Omega_m$ , of 0.3 and a cosmological constant,  $\Omega_\Lambda$ , of 0.7 we have also constructed the REFLEX X-ray luminosity function in the frame of this cosmology. The results are not very different, as shown in Figure 5. But the fitting parameters of the Schechter function yield a notably different value for  $L_*$ , as listed in Table 1. The main difference between the two luminosity functions is that the exponential cutoff is shifted to slightly larger luminosity values in the  $\Omega_\Lambda \neq 0$  model. This is easily understood, because for most of the luminosity range the survey depth is

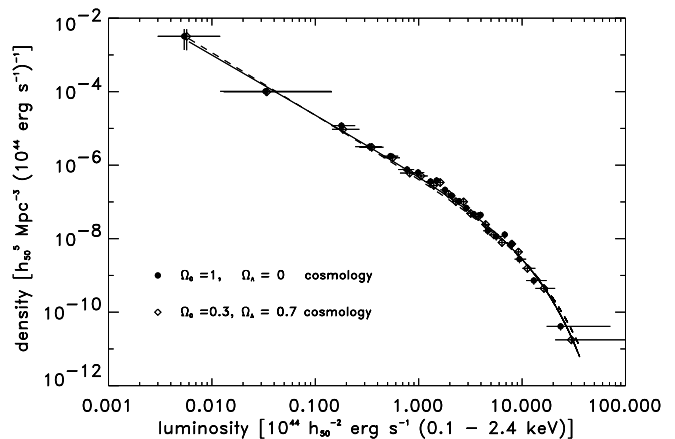


FIG. 5.—Comparison of the REFLEX X-ray luminosity functions derived for Einstein–de Sitter and  $\Lambda$  cosmologies. Data points are corrected for missing flux and both fitted lines are corrected for missing flux and the flux measurement uncertainties. The fit to the  $\Lambda$  cosmology data is shown as a dashed line. The numerical values for the  $\Lambda$  cosmology luminosity function are given in Table 7.

small in cosmological terms and the corrections are negligible. Only for the highest luminosities, where a large fraction of the clusters already have redshifts of the order  $z = 0.3$ , does the correction become apparent.

The effect on the number densities for certain luminosity ranges is moderate, however. To give two typical examples: the integrated number density for  $L_x \geq 5 \times 10^{43}$  ergs  $s^{-1}$  is roughly 10% higher for the critical density universe, and for  $L_x \geq 10^{45}$  ergs  $s^{-1}$  the  $\Lambda$  cosmology yields a number density about 15% higher.

## 7. SUMMARY AND CONCLUSIONS

The REFLEX sample has allowed us to determine the X-ray luminosity function with an accuracy of, for example, better than 25% for 22 independent data bins over 3 orders of magnitude in luminosity (better than 12% for eight independent  $e$ -folding intervals). This accuracy will provide the basis for a precise comparison with luminosity functions determined for high-redshift samples in the search for evolutionary effects. The size of the REFLEX sample has also allowed us to determine the luminosity function of subsamples for different flux limits and different survey regions, to demonstrate the stability of the results. In our forthcoming work, we will use the X-ray luminosity function derived here to obtain constraints on cosmological models.

We thank Joachim Trümper and the *ROSAT* team for providing the RASS data fields and the EXSAS software, as well as H. T. MacGillivray, Daryl Yentis, and the COSMOS team for the digitized optical data. We thank the referee, Bob Nichol, for helpful comments. P. S. and H. B. acknowledge the support by the Verbundforschung under grants 50 OR 9708 35 and 50 OR 93065, respectively.

## APPENDIX A

## DATA TABLES

For the use of these results in cosmological model fitting, we provide in Tables 2–7 the numerical values of the binned representations of the luminosity functions derived in this paper. The parameter  $L_X(\text{cent})$  is the density-weighted mean X-ray luminosity of the clusters in the bin. The errors in the cluster densities are the Poissonian errors based on the number of objects in the bin. Note that we also provide here the REFLEX X-ray luminosity function for the 0.5–2 keV energy band in Table 6.

TABLE 2  
REFLEX X-RAY LUMINOSITY FUNCTION WITHOUT CORRECTION FOR MISSING FLUX

$L_X(\text{cent})^a$ ( $10^{44}$ ergs $s^{-1}$ )	$L_X(\text{max})^a$ ( $10^{44}$ ergs $s^{-1}$ )	$L_X(\text{min})^a$ ( $10^{44}$ ergs $s^{-1}$ )	Density [ $n(L)$ ] [ $h_{50}^5 \text{ Mpc}^{-3} (10^{44} \text{ ergs s}^{-1})^{-1}$ ]	$\Delta n(L)/n(L)$
22.003 .....	59.195	15.243	$4.98 \times 10^{-11}$	0.22
11.964 .....	15.243	10.176	$9.08 \times 10^{-10}$	0.22
8.785 .....	10.176	7.783	$2.86 \times 10^{-9}$	0.22
7.294 .....	7.783	6.649	$7.70 \times 10^{-9}$	0.22
6.209 .....	6.649	5.839	$1.32 \times 10^{-8}$	0.22
5.261 .....	5.839	4.891	$1.41 \times 10^{-8}$	0.22
4.390 .....	4.891	3.982	$1.87 \times 10^{-8}$	0.22
3.697 .....	3.982	3.389	$3.60 \times 10^{-8}$	0.22
3.108 .....	3.389	2.937	$6.00 \times 10^{-8}$	0.22
2.690 .....	2.937	2.481	$7.20 \times 10^{-8}$	0.22
2.290 .....	2.481	2.148	$1.24 \times 10^{-7}$	0.22
1.936 .....	2.148	1.770	$1.36 \times 10^{-7}$	0.22
1.654 .....	1.770	1.505	$2.42 \times 10^{-7}$	0.22
1.395 .....	1.505	1.309	$4.12 \times 10^{-7}$	0.22
1.209 .....	1.309	1.081	$4.32 \times 10^{-7}$	0.22
0.926 .....	1.081	0.826	$5.58 \times 10^{-7}$	0.22
0.715 .....	0.826	0.586	$8.49 \times 10^{-7}$	0.22
0.491 .....	0.586	0.393	$1.80 \times 10^{-6}$	0.22
0.311 .....	0.393	0.213	$3.45 \times 10^{-6}$	0.22
0.163 .....	0.213	0.132	$1.47 \times 10^{-5}$	0.22
0.027 .....	0.132	0.010	$1.09 \times 10^{-4}$	0.22
0.004 .....	0.010	0.002	$3.81 \times 10^{-3}$	0.58

<sup>a</sup> X-ray luminosity in 0.1–2.4 keV band.

TABLE 3  
REFLEX X-RAY LUMINOSITY FUNCTION WITH CORRECTION FOR MISSING FLUX

$L_X(\text{cent})$	$L_X(\text{max})$	$L_X(\text{min})$	$n(L)$
23.572 .....	71.405	17.275	$4.11 \times 10^{-11}$
12.968 .....	17.275	10.941	$7.25 \times 10^{-10}$
9.427 .....	10.941	8.459	$2.77 \times 10^{-9}$
7.985 .....	8.459	7.243	$7.20 \times 10^{-9}$
6.790 .....	7.243	6.417	$1.29 \times 10^{-8}$
5.625 .....	6.417	5.250	$1.15 \times 10^{-8}$
4.656 .....	5.250	4.208	$1.64 \times 10^{-8}$
3.963 .....	4.208	3.721	$4.42 \times 10^{-8}$
3.405 .....	3.721	3.140	$4.66 \times 10^{-8}$
2.887 .....	3.140	2.663	$6.85 \times 10^{-8}$
2.457 .....	2.663	2.267	$1.05 \times 10^{-7}$
2.094 .....	2.267	1.918	$1.47 \times 10^{-7}$
1.797 .....	1.918	1.617	$2.12 \times 10^{-7}$
1.489 .....	1.617	1.403	$3.82 \times 10^{-7}$
1.301 .....	1.403	1.130	$3.59 \times 10^{-7}$
0.987 .....	1.130	0.903	$6.31 \times 10^{-7}$
0.772 .....	0.903	0.633	$7.61 \times 10^{-7}$
0.533 .....	0.633	0.437	$1.76 \times 10^{-6}$
0.336 .....	0.437	0.243	$3.19 \times 10^{-6}$
0.179 .....	0.243	0.143	$1.19 \times 10^{-5}$
0.033 .....	0.143	0.012	$1.02 \times 10^{-4}$
0.005 .....	0.012	0.003	$3.21 \times 10^{-3}$

NOTE.—Units and values for  $\Delta n(L)$  are the same as in Table 2.

TABLE 4  
X-RAY LUMINOSITY FUNCTION FOR THE PART OF THE REFLEX SURVEY  
NORTH OF THE GALACTIC PLANE WITHOUT CORRECTION FOR  
MISSING FLUX

$L_x(\text{cent})$	$L_x(\text{max})$	$L_x(\text{min})$	$n(L)$
17.619 .....	59.195	9.852	$1.48 \times 10^{-10}$
6.896 .....	9.852	5.770	$5.90 \times 10^{-9}$
4.682 .....	5.770	3.786	$2.02 \times 10^{-8}$
2.839 .....	3.786	2.222	$5.01 \times 10^{-8}$
1.802 .....	2.222	1.463	$1.93 \times 10^{-7}$
1.289 .....	1.463	1.074	$5.99 \times 10^{-7}$
0.616 .....	1.074	0.429	$9.89 \times 10^{-7}$
0.113 .....	0.429	0.033	$1.25 \times 10^{-5}$
0.014 .....	0.033	0.006	$1.41 \times 10^{-3}$

NOTE.—Units are the same as in Table 2, and  $\Delta n(L)$  has a value of 25% (for 16 clusters per bin), except for the last bin, where the value is 41%.

TABLE 5  
X-RAY LUMINOSITY FUNCTION FOR THE PART OF THE REFLEX SURVEY  
SOUTH OF THE GALACTIC PLANE WITHOUT CORRECTION FOR  
MISSING FLUX

$L_x(\text{cent})$	$L_x(\text{max})$	$L_x(\text{min})$	$n(L)$
16.441 .....	46.892	12.609	$1.04 \times 10^{-10}$
10.152 .....	12.609	9.005	$1.83 \times 10^{-9}$
7.995 .....	9.005	7.293	$5.23 \times 10^{-9}$
6.642 .....	7.293	6.073	$9.36 \times 10^{-9}$
5.449 .....	6.073	4.976	$1.35 \times 10^{-8}$
4.316 .....	4.976	3.939	$1.94 \times 10^{-8}$
3.546 .....	3.939	3.241	$3.76 \times 10^{-8}$
3.002 .....	3.241	2.826	$7.93 \times 10^{-8}$
2.576 .....	2.826	2.349	$8.47 \times 10^{-8}$
2.178 .....	2.349	1.991	$1.43 \times 10^{-7}$
1.761 .....	1.991	1.640	$1.93 \times 10^{-7}$
1.462 .....	1.640	1.317	$2.74 \times 10^{-7}$
1.149 .....	1.317	0.997	$3.81 \times 10^{-7}$
0.870 .....	0.997	0.774	$8.09 \times 10^{-7}$
0.628 .....	0.774	0.521	$1.12 \times 10^{-6}$
0.389 .....	0.521	0.322	$2.72 \times 10^{-6}$
0.209 .....	0.322	0.153	$6.33 \times 10^{-6}$
0.018 .....	0.153	0.004	$1.39 \times 10^{-4}$
0.003 .....	0.004	0.002	$1.26 \times 10^{-2}$

NOTE.—Units are the same as in Table 2, and  $\Delta n(L)$  has a value of 25%, except for the last bin, where the value is 100%.

TABLE 6  
REFLEX X-RAY LUMINOSITY FUNCTION FOR THE 0.5–2 KEV ENERGY BAND,  
WITH CORRECTION FOR MISSING FLUX

$L_x(\text{cent})$	$L_x(\text{max})$	$L_x(\text{min})$	$n(L)$
14.760 .....	44.712	10.810	$6.57 \times 10^{-11}$
8.109 .....	10.810	6.833	$1.16 \times 10^{-9}$
5.881 .....	6.833	5.274	$4.40 \times 10^{-9}$
4.977 .....	5.274	4.513	$1.15 \times 10^{-8}$
4.230 .....	4.513	3.997	$2.07 \times 10^{-8}$
3.501 .....	3.997	3.267	$1.83 \times 10^{-8}$
2.898 .....	3.267	2.619	$2.63 \times 10^{-8}$
2.463 .....	2.619	2.310	$6.97 \times 10^{-8}$
2.114 .....	2.310	1.949	$7.51 \times 10^{-8}$
1.792 .....	1.949	1.653	$1.10 \times 10^{-7}$
1.522 .....	1.653	1.405	$1.66 \times 10^{-7}$
1.294 .....	1.405	1.185	$2.34 \times 10^{-7}$

TABLE 6—Continued

$L_x(\text{cent})$	$L_x(\text{max})$	$L_x(\text{min})$	$n(L)$
1.111 .....	1.185	0.999	$3.44 \times 10^{-7}$
0.920 .....	0.999	0.867	$6.17 \times 10^{-7}$
0.804 .....	0.867	0.696	$5.75 \times 10^{-7}$
0.608 .....	0.696	0.556	$1.02 \times 10^{-6}$
0.476 .....	0.556	0.390	$1.23 \times 10^{-6}$
0.328 .....	0.390	0.270	$2.88 \times 10^{-6}$
0.209 .....	0.270	0.162	$5.73 \times 10^{-6}$
0.119 .....	0.162	0.096	$1.78 \times 10^{-5}$
0.024 .....	0.096	0.009	$1.54 \times 10^{-4}$
0.004 .....	0.009	0.002	$4.51 \times 10^{-3}$

NOTE.—Units and values for  $\Delta n(L)$  are the same as in Table 2.

TABLE 7

REFLEX X-RAY LUMINOSITY FUNCTION WITH CORRECTION FOR MISSING FLUX  
FOR A COSMOLOGY CHARACTERIZED BY THE PARAMETERS  $\Omega_0 = 0.3$   
AND  $\Omega_\Lambda = 0.7$

$L_x(\text{cent})$	$L_x(\text{max})$	$L_x(\text{min})$	$n(L)$
29.946 .....	106.152	20.876	$1.77 \times 10^{-11}$
16.274 .....	20.876	13.441	$4.44 \times 10^{-10}$
11.250 .....	13.441	10.063	$1.56 \times 10^{-9}$
9.211 .....	10.063	8.468	$4.36 \times 10^{-9}$
7.938 .....	8.468	7.299	$7.19 \times 10^{-9}$
6.391 .....	7.299	5.896	$7.87 \times 10^{-9}$
5.338 .....	5.896	4.792	$1.27 \times 10^{-8}$
4.440 .....	4.792	4.041	$2.43 \times 10^{-8}$
3.767 .....	4.041	3.468	$4.01 \times 10^{-8}$
3.185 .....	3.468	2.892	$4.87 \times 10^{-8}$
2.718 .....	2.892	2.539	$1.01 \times 10^{-7}$
2.288 .....	2.539	2.095	$1.02 \times 10^{-7}$
1.947 .....	2.095	1.751	$1.64 \times 10^{-7}$
1.614 .....	1.751	1.536	$3.39 \times 10^{-7}$
1.398 .....	1.536	1.223	$2.81 \times 10^{-7}$
1.053 .....	1.223	0.966	$5.09 \times 10^{-7}$
0.819 .....	0.966	0.659	$6.11 \times 10^{-7}$
0.560 .....	0.659	0.457	$1.59 \times 10^{-6}$
0.351 .....	0.457	0.267	$3.08 \times 10^{-6}$
0.185 .....	0.267	0.145	$9.45 \times 10^{-6}$
0.034 .....	0.145	0.013	$9.90 \times 10^{-5}$
0.0057 .....	0.013	0.003	$3.18 \times 10^{-3}$

NOTE.—Units and values for  $\Delta n(L)$  are the same as in Table 2.

## REFERENCES

- Abell, G. O., Corwin, H. G., Jr., & Olowin, R. P. 1989, *ApJS*, 70, 1  
 Anders, E., & Grevesse, N. 1989, *Geochim. Cosmochim. Acta*, 53, 197  
 Bahcall, N. A., & Cen, R. 1993, *ApJ*, 407, L49  
 Böhringer, H., et al. 1998, *Messenger*, 94, 21  
 ———, 2000, *ApJS*, 129, 435  
 ———, 2001, *A&A*, 369, 826 (Paper I)  
 Borgani, S., Rosati, P., Tozzi, P., & Norman, C. 1999, *ApJ*, 517, 40  
 Burke, D. J., Collins, C. A., Sharples, R. M., Romer, A. K., Holden, B. P., & Nichol, R. C. 1997, *ApJ*, 488, L83  
 Burns, J. O., Ledlow, M. J., Loken, C., Klypin, A., Voges, W., Bryan, G. L., Norman, M. L., & White, R. A. 1996, *ApJ*, 467, L49  
 Cavaliere, A., & Fusco-Femiano, R. 1976, *A&A*, 49, 137  
 Collins, C. A., Burke, D. J., Romer, A. K., Sharples, R. M., & Nichol, R. C. 1997, *ApJ*, 479, L117  
 Collins, C. A., et al. 2000, *MNRAS*, 319, 939 (Paper II)  
 Daley, D. J., & Vere-Jones, D. 1988, *An Introduction to the Theory of Point Processes* (New York: Springer)  
 De Grandi, S., et al. 1999, *ApJ*, 513, L17  
 Dickey, J. M., & Lockman, F. J. 1990, *ARA&A*, 28, 215  
 Ebeling, H., Edge, A. C., Fabian, A. C., Allen, S. W., Crawford, C. S., & Böhringer, H. 1997, *ApJ*, 479, L101  
 Eddington, A. S. 1940, *MNRAS*, 100, 354  
 Edge, A. C., Stewart, G. C., Fabian, A. C., & Arnaud, K. A. 1990, *MNRAS*, 245, 559  
 Eke, V. R., Cole, S., & Frenk, C. S. 1996, *MNRAS*, 282, 263  
 Gioia, I. M., Henry, J. P., Mullis, C. R., Voges, W., Briel, U. G., Böhringer, H., & Huchra, J. P. 2001, *ApJ*, 553, L105  
 Gioia, I. M., Maccacaro, T., Schild, R. E., Stocke, J. T., Liebert, J. W., Danziger, I. J., Kunth, D., & Lub, J. 1984, *ApJ*, 283, 495  
 Guzzo, L., et al. 1999, *Messenger*, 95, 27  
 Henry, J. P., & Arnaud, K. A. 1991, *ApJ*, 372, 410  
 Henry, J. P., Gioia, I. M., Maccacaro, T., Morris, S. L., Stocke, J. T., & Wolter, A. 1992, *ApJ*, 386, 408  
 Kowalski, M. P., Ulmer, M. P., Cruddace, R. G., & Wood, K. S. 1984, *ApJS*, 56, 403  
 Ledlow, M. J., Loken, C., Burns, J. O., Owen, F. N., & Voges, W. 1999, *ApJ*, 516, L53  
 MacGillivray, H. T., & Stobie, R. S. 1984, *Vistas Astron.*, 27, 433  
 Markevitch, M. 1998, *ApJ*, 504, 27  
 Murdoch, H. S., Crawford, D. F., & Jauncey, D. L. 1973, *ApJ*, 183, 1  
 Nichol, R. C., et al. 1999, *ApJ*, 521, L21  
 Oukbir, J., & Blanchard, A. 1992, *A&A*, 262, L21

- Perrenod, S. C. 1980, *ApJ*, 236, 373
- Piccinotti, G., Mushotzky, R. F., Boldt, E. A., Holt, S. S., Marshall, F. E., Serlemitsos, P. J., & Shafer, R. A. 1982, *ApJ*, 253, 485
- Raymond, J. C., & Smith, B. W. 1977, *ApJS*, 35, 419
- Reichart, D. E., Nichol, R. C., Castander, F. J., Burke, D. J., Romer, A. K., Holden, B. P., Collins, C. A., & Ulmer, M. P. 1999, *ApJ*, 518, 521
- Reiprich T. H., & Böhringer, H. 1999, *Astron. Nachr.*, 320, 296
- . 2001, *ApJ*, in press
- Rosati, P., Della Ceca, R., Norman, C., & Giacconi, R. 1998, *ApJ*, 492, L21
- Schechter, P. 1976, *ApJ*, 203, 297
- Schuecker, P., et al. 2001, *A&A*, 368, 86 (Paper III)
- Trümper, J. 1992, *QJRAS*, 33, 165
- . 1993, *Science*, 260, 1769
- Viana, P. T. P., & Liddle, A. R. 1996, *MNRAS*, 281, 323
- Vikhlinin, A., McNamara, B. R., Forman, W., Jones, C., Quintana, H., & Hornstrup, A. 1998, *ApJ*, 498, L21
- Voges, W., et al. 1999, *A&A*, 349, 389
- White, S. D. M., Efstathiou, G., & Frenk, C. S. 1993, *MNRAS*, 262, 1023
- Zimmermann, H.-U., Becker, W., Belloni, T., Döbereiner, S., Izzo, C., Kahabka, P., & Schwentker, O. 1994, *EXSAS User's Guide* (4th ed.; MPE Rep. 257; Garching: MPE)